The Use of Neural Networks and Texture Analysis for Rapid Objective Selection of Regions of Interest in Cytoskeletal Images

Amanda D. Felder Derkacs,[1] Samuel R. Ward,[2] and Richard L. Lieber[3,*]

[1]Department of Bioengineering, University of California-San Diego, 9500 Gilman Drive, La Jolla, CA 92093-0863, USA
[2]Departments of Radiology, Orthopaedic Surgery, and Bioengineering, University of California-San Diego,
 9500 Gilman Drive, La Jolla, CA 92093-0610, USA
[3]Departments of Orthopaedic Surgery and Bioengineering, V.A. Medical Center, University of California-San Diego,
 9500 Gilman Drive, La Jolla, CA 92093-0863, USA

Abstract: Understanding cytoskeletal dynamics in living tissue is prerequisite to understanding mechanisms of injury, mechanotransduction, and mechanical signaling. Real-time visualization is now possible using transfection with plasmids that encode fluorescent cytoskeletal proteins. Using this approach with the muscle-specific intermediate filament protein desmin, we found that a green fluorescent protein–desmin chimeric protein was unevenly distributed throughout the muscle fiber, resulting in some image areas that were saturated as well as others that lacked any signal. Our goal was to analyze the muscle fiber cytoskeletal network quantitatively in an unbiased fashion. To objectively select areas of the muscle fiber that are suitable for analysis, we devised a method that provides objective classification of regions of images of striated cytoskeletal structures into "usable" and "unusable" categories. This method consists of a combination of spatial analysis of the image using Fourier methods along with a boosted neural network that "decides" on the quality of the image based on previous training. We trained the neural network using the expert opinion of three scientists familiar with these types of images. We found that this method was over 300 times faster than manual classification and that it permitted objective and accurate classification of image regions.

Key words: image analysis, classification, skeletal muscle, confocal microscopy

INTRODUCTION

The cellular cytoskeleton has emerged as a multifunctional organelle that serves not only to maintain cell shape and strength, but is capable of performing transducer functions such as activating cellular signaling cascades that ultimately result in altered gene expression (Gautel, 2011). This function often occurs in a background of cell growth and division, which means that the assembly and disassembly of the cytoskeleton must be relatively rapid (Kueh et al., 2010) and robust. Indeed, recent studies have identified heretofore unexpectedly rapid turnover of cytoskeletal structures that conclusively demonstrate the dynamic nature of the cytoskeleton (Imanaka-Yoshida et al., 1993). Often real-time analysis of cytoskeletal structures involves methods in which cytoskeletal fusion proteins are expressed in living cells and tissues and then imaged by confocal microscopy.

To determine the optimal timing of tissue harvest after transfection with a fusion protein, prior studies in our group have examined protein expression and contractile function of muscle over a 28-day period post–green fluorescent protein (GFP) plasmid transfection (Palmisano et al., 2007). Briefly, the amount of GFP protein present in transfected tissue was determined by Western blot. The protein was transiently expressed, peaking 7 days after transfection

and becoming nearly undetectable after 28 days. Additionally, maximal isometric force generation of the mouse hindlimb (Barash et al., 2004) was used to evaluate the effects of the transfection on the muscle's function. Isometric force had diminished the most at 1 and 3 days, but by 21 days force had returned to pretransfection values. About 65% of the force had been regained at 7 days, which was significantly more that at 3 days.

One of the challenges in performing analysis of such dynamic cellular images is selecting the region of interest (ROI) to be analyzed. Clearly millions of such ROIs are available within large samples, and the temptation is to be attracted to ROIs based on preconceived notions of cell structures or the process studied. This manual selection process may yield biased and, therefore, incorrect results (Eilbert et al., 1990). In addition, manual selection of ROIs can be extremely time-consuming, which limits the total volume fraction of tissue that can be analyzed and thus the generalizability of the results because a small volume fraction of the tissue is probed (Weibel, 1980). Thus, creating a method that rapidly and objectively selects valid ROIs (i.e., ROIs that meet the researcher's expert criteria) would be very valuable.

Texture and structure analyses are methods commonly used to distinguish one area of an image from another (Kayser et al., 2009). Texture analysis examines the pixel-based distribution of gray values within an image whereas
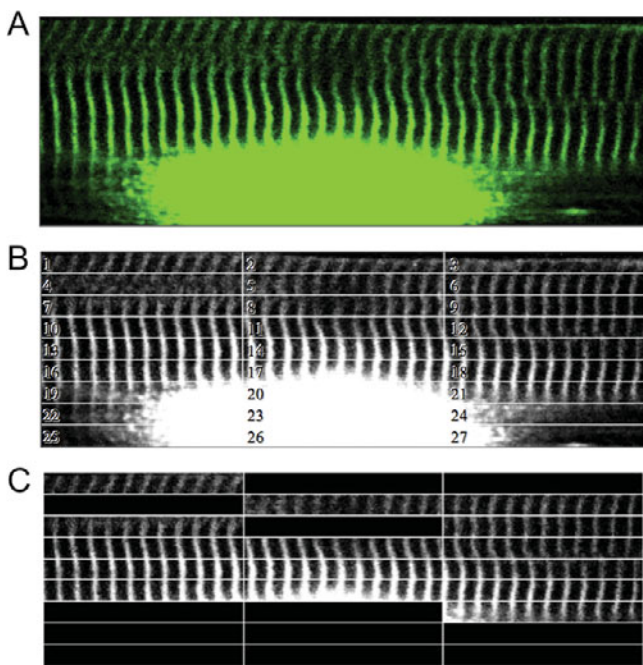
Figure 1. Confocal images from a skeletal muscle fiber expressing the GFP-desmin chimeric protein. **A:** Typical image of a GFP-desmin-transfected fiber. There is oversaturation around the nucleus, while other regions contain low levels of expression. **B:** Partitioning of original image into 27 sections for analysis. FFT and non-FFT parameters were calculated within each section and used for classifying. **C:** Results of classification performed by trained neural network. Blackened sections were classified as "unusable," while the remaining sections were classified as "usable" for further analysis. Regions of oversaturation as well as regions with low signal were eliminated by the network.

structure analysis is based on the identification and spatial positioning of objects. Simple measurements of texture can be obtained by observing the distribution of neighboring pixels' gray values around each pixel and calculating metrics based on their frequencies of co-occurrence (Haralick, 1979). Other metrics are based on the frequency of edges within an image area and runs of neighboring pixels with similar gray values. These simple metrics are referred to as statistical measures of texture. Other measures of texture can be obtained from a number of operations, including local linear transforms (Unser, 1986), wavelet transforms (Unser, 1995), Fourier transforms (Desoky & Hall, 1990; Zou & Wang, 2001), discrete cosine tranforms (Desoky & Hall, 1990), and Hadamard transforms (Desoky & Hall, 1990).

When working with images of longitudinally-oriented skeletal muscle fibers, it is possible to exploit their regular structure to identify areas of interest. The spatial regularity of cytoskeletal proteins reflects the longitudinally-oriented sarcomere structures within muscle fibers (Fig. 1A). While edge detection can be used to define sarcomere length (Infantolino et al., 2010), the longitudinal regularity of muscle is especially suited for analysis by Fourier transform (Shah & Lieber, 2003). The one-dimensional fast Fourier transform (FFT) has been most often used to find the

dominant frequency in high-quality images, which corresponds to the sarcomere length (Gannier et al., 1993; Helmes et al., 1999; Weiwad et al., 2000; Ockleford et al., 2002; Shah & Lieber, 2003), although the FFT-derived power spectrum also provides information on the relative strength of that frequency and may help determine whether an ROI is acceptable by quantifying how clear repeating structures are in that region.

Texture and structural measures calculated from ROIs can be used to sort regions into two or more classifications. Common classification methods include multivariate analysis, logistical regression, and neural networks. These approaches typically implement a set of training images that has already been classified by an expert to initially "construct" the classifier. The power of these classification algorithms is that, from the training set of images, they can determine the quantifiable characteristics of an image that factor into the classification and even their relative importance in determining the classification. Once constructed, the classifier can then classify new images based on their texture or feature measures, usually hundreds or thousands of times faster than manual processing, and in an unbiased fashion. In this article, we describe a method to select ROIs from confocal images of striated cytoskeletal structures. A neural network reproduced investigators' decisions by using statistical and spatial-frequency-based measures of texture to select areas of the image with strong signal, with low noise, and without oversaturation. This method would allow objective analysis of how cytoskeletal structures change during a bout of isometric or eccentric exercise in future studies.

MATERIALS AND METHODS

Experimental Model

Experiments were performed on the fifth toe of the extensor digitorum longus (EDL) muscle from wild-type 129/Sv (Taconic Farms, Germantown, NY, USA) and desmin-null 129/Sv (Milner et al., 1996) mice. All procedures were performed in accordance with the National Institutes of Health (NIH) Guide for the Use and Care of Laboratory Animals and were approved by the University of California and Department of Veteran's Affairs Committees on the Use of Animal Subjects in Research. The EDL was injected either with plasmid DNA encoding a GFP-desmin chimeric protein or a mix of plasmids encoding GFP-desmin and red fluorescent protein (RFP)-α-actinin, and the plasmids were introduced into the cells by electroporation with a mouse-specific TriGrid Delivery System (IChor Medical Systems, Inc., San Diego, CA, USA) (Vitadello et al., 1994).

Experiments reported here were performed on muscles 7 days after transfection, as we could be confident in adequate protein expression and muscle function at this time-point (Palmisano et al., 2007). Immediately after sacrifice, hindlimbs were skinned, transected, and placed in chilled mammalian Ringer's solution. The fifth-toe EDL muscle belly was removed with its tendons intact and was checked

for chimeric protein expression under a dissecting scope (Model MZ-16, Leica, Wetzlar, Germany) by fluorescent illumination. Muscles with little or no transfection or muscles with transfection only in the center of the tissue (which would preclude epi-illumation confocal microscopy) were excluded from further analysis. A total of 8 muscles having sufficient transfection were used in this study.

Confocal Microscopy

Intact muscle fibers within whole muscles were viewed using a Zeiss LSM 510 confocal microscope with a 40×/0.6 LD Plan-Neofluar objective, which has a working distance of 2.9 mm. With the Ar-Kr laser power set to 50%, twelve 512 × 512 pixel image stacks (7 images, 1 μm spacing, 2× line averaging, scan speed of 8, 2.0× zoom) of the same region were taken in 3-min intervals. All imaging parameters (pinhole size, gain, and offset) were optimized for the first image and were not adjusted for the remainder of the experiment. Focus was adjusted as needed to keep the selected portion of the fiber in focus.

Since susceptibility of GFP to photobleaching represents a potentially confounding variable in analysis of the image series, we performed pilot experiments using photobleaching controls without any muscle contraction. The results of these pilot studies demonstrated that a scan speed of 8 and stack size of 7 images produced excellent images of adequate image brightness that yielded a large image stack that included approximately 93,000 μm^3 of muscle fiber volume.

Image Processing

Single images from each stack in an experimental series from the same optical plane were manually identified and used for further analysis. Images were first manually rotated if necessary so that a single fiber expressing GFP-desmin or RFP-α-actinin was aligned with the image panel. Then, in an automated fashion, image translations were defined using a hierarchical motion estimation algorithm (Bergen et al., 1992); the reverses of the translations were applied to the series to re-align the images; and finally, the image series was cropped to include the largest region that all images contained. A sample of an unaligned sequence of images and an aligned sequence is provided as Supplementary Movie 1.

Supplementary Movie 1

Supplementary Movie 1 can be found online. Please visit journals.cambridge.org/jid_MAM.

Image Analysis

The following analysis was automatically performed across the stack of images: Each image was portioned into smaller rectangular sections such that each section covered one-third of the image width and was 18 pixel rows high (Fig. 1A). This partitioned the image into roughly 30 sections—arranged 3 across and ~10 high. Fourier trans-

Table 1. Parameters Obtained from Each Image Section.

FFT-Derived Parameters	Statistical and Other Parameters
Peak power	Brightness
Peak power variance	Percentage of saturated pixels
Peak power width	Percentage of pixels with no signal
Noise	Entropy
Power-to-noise ratio	Horizontal contrast
Sarcomere length	Vertical long run statistic
Sarcomere length variance	
Phase shift	
Phase shift variance	
Percentage of rows with reasonable SL	

form tools were applied to each section along the pixel rows (from 150 to 170 pixels long) to quantify optical power, power variance, power peak width, sarcomere length, sarcomere length variance, myofibrillar phase shift (Shah et al., 2004), phase shift variance, noise, and power-to-noise. Other parameters calculated were image brightness, saturated and unsaturated pixel percentages, as well as several statistical measures of texture (Table 1).

Calculation of Parameters from the FFT

Prior to Fourier analysis, the pixel rows of each image segment were autocorrelated. The autocorrelation function A_F at point i over a window size of $2w + 1$ is given by

$$A_F(m) = \frac{\sum_{u=i-w}^{i+w} F(u)F(u-m)}{N - m} \quad (1)$$

for $-w \leq m \leq w$ pixel lags, where $F(u)$ is the intensity profile of the segment row and N is the row width. The autocorrelation amplified the intensity profile by a power of two at its peaks, resulting in increased signal-to-noise ratio compared to the raw intensity profile (Shah & Lieber, 2003). The power spectrum from each autocorrelated segment row was then calculated from the 1,024-point FFT.

$$X(k) = \frac{\sum_{m=0}^{M-1} A_F(m)e^{(2\pi j/M)km}}{M} \quad \text{for } k = (0,1,\ldots,M-1),$$

$$(2)$$

where j is the imaginary unit, and $M = 2w + 1$.

Peak power for each segment row was determined from the power spectrum. Power width was determined as the width of the power peak at one-tenth of the peak power value. Noise was determined as the average power value at frequencies above 1 μm^{-1}. This frequency cutoff was selected because noise contributes greatly to the power at these high spatial frequencies, whereas our structures of interest (Z-disks) have a relatively low spatial frequency. A power-to-noise ratio was calculated by dividing the peak power value by the calculated noise value. Since the fusion proteins were located at the muscle Z-disk, sarcomere length

was determined from each segment row as the reciprocal of the peak frequency of the power spectrum. All parameters were averaged across each image section; peak power variance and sarcomere length variance were determined from the row segment values within each image section.

Phase shift between adjacent myofibrils within the sarcomere lattice was quantified by first calculating the pixel offsets between peaks of autocorrelated intensity profiles of rows 0.6 μm apart (approximating myofibrillar diameter). Then, the variance of the mean phase shift for all myofibrils in each section was also calculated. This value has been used as a measure of myofibrillar "connectivity" because a sarcomere lattice with high connectivity yields a low variance (Shah & Lieber, 2003).

Calculation of Texture Statistics and Other Parameters

Saturated and unsaturated pixel percentages for each image section were calculated as the percent of total pixels in each image section that had the gray value of 255 or 0, respectively. Before calculating entropy and contrast, image pixel values were quantized to 16 gray levels. The vertical co-occurrence matrix C_V was then calculated for each image section as follows: C_{Vij} is the number of times a pixel of gray level i is positioned directly above a pixel of gray level j within the image section. The horizontal co-occurrence matrix C_H was calculated in a similar manner. Entropy (a measure of randomness in the image's pixels) was then defined as

$$-\sum_i \sum_j C_{Vij} \log C_{Vij}. \tag{3}$$

Vertical contrast (a measure of the difference between vertically adjacent pixels' brightness) was calculated as

$$\sum_i \sum_j (i-j)^2 C_{Vij}. \tag{4}$$

The horizontal contrast can be calculated in a similar manner using the horizontal co-occurrence matrix C_H in place of C_V. To determine the vertical long run statistic (a measure of vertically-oriented strings of pixels of similar brightness), the vertical run matrix P was first calculated, where P_{ij} is the number of times there is a run of length j in the vertical direction having the same quantized gray tone i. The vertical long run emphasis statistic was then calculated as

$$\frac{1}{T} \sum_{i=1}^{G} \sum_{j=1}^{R} j^2 P_{ij}, \tag{5}$$

where T is the total number of runs, G is the number of gray tones (16), and R is the length of the longest run.

To distinguish objectively among areas with usable information and those with noise, saturation, or no fiber, a neural network was created to objectively classify areas as "to be analyzed/valid" and "not to be analyzed/invalid." All parameters described above (Table 1) were calculated for each image section and were entered into the network. One
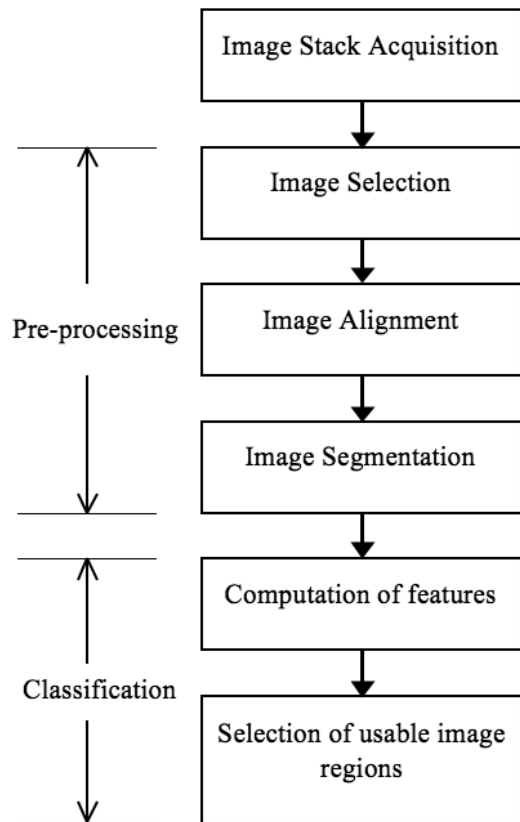
Figure 2. Flow diagram of image classification. Preprocessing steps include image selection from the acquired stack, automated image alignment to adjust for translation, and image segmentation. Classification steps include the computation of parameter values within each image segment and application of the network to select the usable image regions.

hundred twenty-six image sections from four images of varying quality were used to train the network. Three investigators, each a skeletal muscle researcher experienced with confocal microscopy, ranked each section as very poor, poor, good, or very good. Comparison of the investigators' rankings produced weighted kappa values between 0.78 and 0.90, indicating very good to excellent agreement (Portney & Watkins, 1993). The network's training data consisted of the investigators' averaged classifications for each image section along with each section's imaging data. The classifying network was trained in Matlab by employing an adaptation of the Real AdaBoost algorithm from the GML Matlab Toolbox (MSU Graphics & Media Lab, Computer Vision Group, http://graphics.cs.msu.ru) (Freund & Schapire, 1996), using 150 weak learners (iterations) with a single-split classification structure. An overview of the steps involved in image processing and analysis can be found in Figure 2.

RESULTS

The ability of a neural network to "learn" the basis for the expert classification can be determined by following the error in classification of each image by the network as a function of the number of times the network iterates.
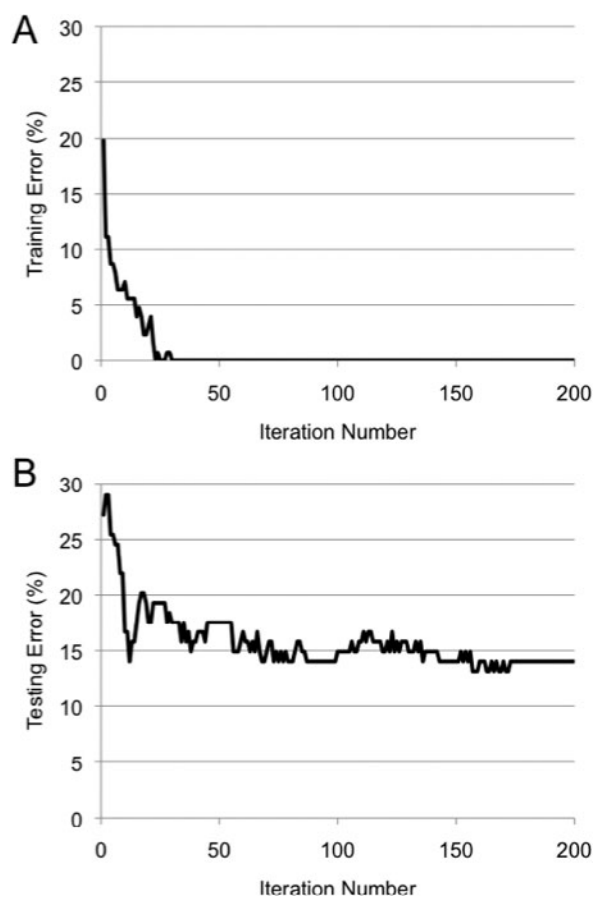
Figure 3. Error of the classification network. **A:** Training error as a function of iteration number. Training error decreases rapidly to zero within 35 iterations and remains stable with further iterations. **B:** Testing error of the classification network as a function of iteration number on a novel set of 114 images, used to evaluate network performance. Error dropped to below 15% after 150 iterations and remained stable thereafter.

During network training, error dropped to 0% by 30 iterations and remained stable with further iterations (Fig. 3A), which indicates that the network "learned" what constitutes a usable ROI. The network's performance was then tested on 114 novel image sections by comparing network-defined and user-defined classifications. The error on the evaluation set of images dropped to below 15% by 150 iterations (Fig. 3B). Increasing the complexity of the network by either adding iterations or by using a higher-order decision tree did not improve error percentage. Thus we chose a classification network of the simplest structure with 150 iterations. For all image sections in this evaluation set, the network correctly matched the investigators' averaged input 86% of the time. However, for image sections that were user-classified as very good or very poor, the network performed extremely well, with 100% and 96% agreement, respectively.

Implementation of the trained network was fast, taking less than a second to classify approximately 250 regions contained within a 10-image set. This is 300 times faster than the manual method, which required about 5 min. The network successfully removed areas with oversaturation,
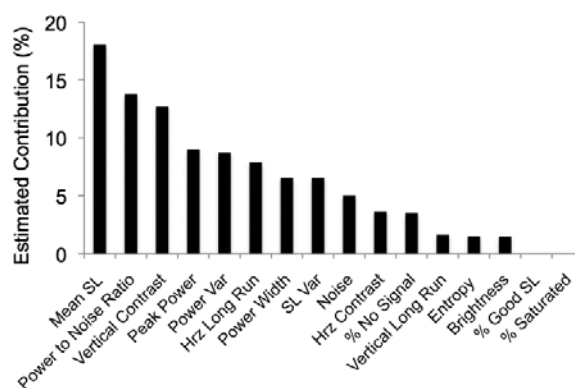
Figure 4. Relative contribution of different parameters to the network's classification decisions. Mean sarcomere length (Mean SL), power-to-noise ratio, and vertical contrast were the most important parameters and together accounted for 45% of the basis of the classification. Note that the percent of rows that were at a reasonable sarcomere length (% Good SL), and the percent of pixels that were saturated (% Saturated) did not contribute to the network's classification. Hrz, horizontal; SL, sarcomere length; Var, variation; Vrt, vertical.

high noise levels, and lack of signal. We observed the actual "choices" of ROIs selected by the network to determine the intuitive basis for these signals. For the GFP-desmin plasmid, the Z-bands and the myonuclei within the fiber are heavily labeled (Fig. 1B). The regions that were classified as unfit for further analysis are blacked out in Figure 1C. It is clearly seen that, after processing, the saturated ROIs around the myonucleus (Fig. 1C; regions 19, 20, 22–27) were eliminated. Regions with insufficient periodicity (and therefore low Fourier periodicity) were also eliminated (Fig. 1C; regions 2–4, 8).

The relative importance that each of the various parameters plays in training the network's classification of image sections was estimated by separating the iterations by parameter and totaling the absolute value of their weights (Fig. 4). The three most important factors in the trained network's classification were mean sarcomere length, power-to-noise ratio (a measure of the Z-disk signal compared to high-frequency noise), and vertical contrast (a measure of difference in brightness between vertically adjacent pixels). On the other hand, the percent of rows that were at a reasonable sarcomere length and the percent of pixels that were saturated did not contribute to the network's classification. While these parameters might have entered into the classification scheme if a larger number of training iterations (weak learners) had been used, they would not have contributed to improving the classification because we had determined that more iterations did not improve the network's performance.

We also tested the network's susceptibility to error due to image selection and focus errors, two potential confounding sources of variation. First, the importance of selecting the correct image from the stack to capture the same focal plane was determined (Fig. 5A). Successive image stacks were obtained of a transfected fiber in a relaxed muscle. In

(a)

(b)
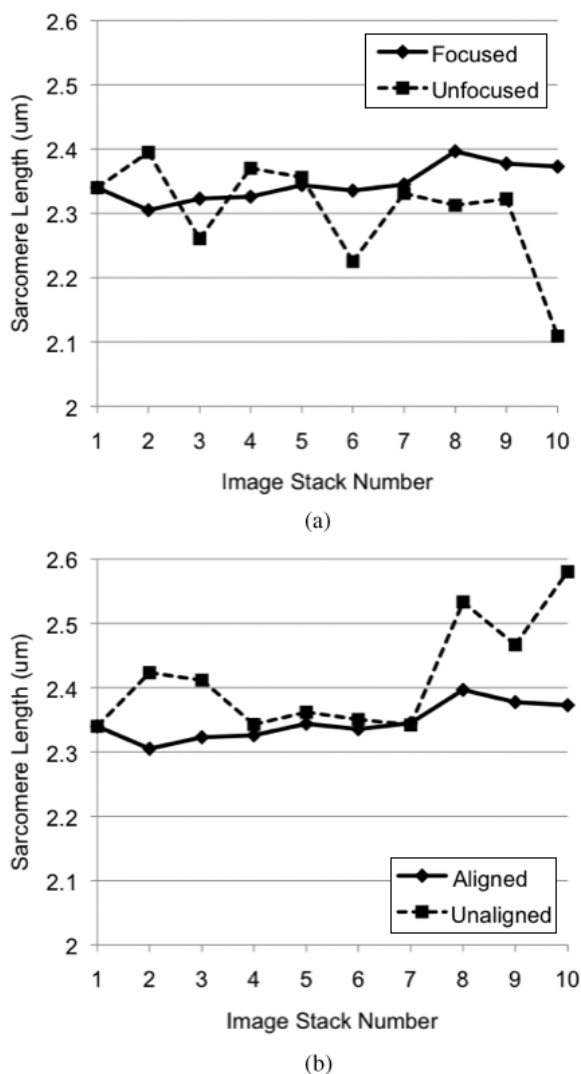
Figure 5. Effects of preprocessing of image stacks. Sarcomere length versus image stack number was calculated from images of a fiber from a relaxed muscle. Since the muscle was not moved during the experiment, the sarcomere length should not change. **A:** The importance of selecting images from the same focal plane. The unfocused image set consisted of the middle image of each stack, while the focused images were identified by eye as being from the same focal plane and were not necessarily in the same location in each stack. Note that the sarcomere length remains relatively constant when the image series is taken from the same focal plane. **B:** The importance of aligning images. Both sets of images were selected to be in the same focal plane. The unaligned images were all cropped in the same way as the first aligned image, yielding images of the same size. Note that aligning images removes much of the variation in sarcomere length.

the "focused" set, one image from each stack was selected by hand so that the same focal plane was followed across the stacks. In the "unfocused" set, the middle image from each stack was selected for further analysis. Both sets of images were aligned and cropped, and the first image in the focused set was classified by the neural network. The regions classified as good in this image were analyzed for all other images in both sets. We examined the sarcomere length from each

image set to gauge the importance of selecting images from the same focal plane. In the resulting sarcomere length versus image stack number (Fig. 5A), sarcomere length should remain constant over the set of image stacks because the muscle was not moved during the experiment. Additionally, sarcomere length should not change should any photobleaching occur with repeated imaging, whereas other texture measures based on pixel gray values may. While it does remain relatively constant for the focused images (coefficient of variation = 1.2%), it changes substantially in the unfocused set of images (coefficient of variation = 3.7%), demonstrating the importance of using images from the same focal plane.

Likewise, the importance of image alignment was defined from image stacks obtained from a fiber in a relaxed muscle (Fig. 5B). This time, only images from the same focal plane were used. However, in the "unaligned" set, the images were not aligned to adjust for any translation, but were only cropped to yield the same sized images as in the "aligned" set. The first image of the aligned set was used to identify good areas in all other images for further analysis. The sarcomere length of the unaligned images was unstable (coefficient of variation = 3.6%), while the sarcomere length from the aligned images remains relatively constant (coefficient of variation = 1.2%), throughout the series of stacks.

Discussion

In this study, we have exploited the use of engineered vectors introduced into living tissue by transfection to track and image chimeric cytoskeletal proteins. However, uptake and expression of injected plasmid can be nonuniform, resulting in irregular expression of the chimeric protein. Within a single fiber from a transfected muscle, there are regions that have high expression of the protein and other regions with no expression at all. This is in contrast to the uniform labeling achievable with standard immunohistochemistry. Our classification method performed automated selection of ROIs within sections based on measured parameters within the image and training against expert opinion.

Our classification process (Fig. 2) was automated and did not require additional input from an investigator. However, images from the same focal plane were manually selected from successive confocal stacks during image preprocessing. Our classification method proved accurate as it agreed with the investigators' classifications over 85% of the time. Furthermore, it was over 300 times faster than manual classification and allowed for objective selection of high-quality regions of the fiber images for further study. This increase in speed and automation will permit a greater sampling of the tissue than would be possible with a slower process. This classification process is somewhat limited in that it requires images to have certain properties, specifically a fixed resolution (in the current article, this was 4.4 pixels/μm) and a minimum image width of 150 pixels. Aside from those properties, there were no further specifications required for an image to be classified with our method. It should be noted

that our setup and many of our imaging parameters remained the same for all images (see the Confocal Microscopy section), so it is likely that this allowed our image quality to be relatively consistent across different image stacks.

Image classification schemes have been previously used to study skeletal muscle. The task of discerning muscle fibers from other cells and fascia in images of muscle cross sections and fascia is commonly performed in muscle studies. Simple thresholding is still used, but more advanced methods such as active contours have recently been proposed. Image areas from skeletal muscle cross sections have been classified for semiautomatic or automatic computation of muscle fiber areas, perimeter and diameter, using active contours alone (Klemenčič et al., 1998), or in combination with texture and color features (Kim et al., 2007). Advanced edge-detection methods have also be used to automate this computation on images of skeletal muscle cross sections (Tzekis et al., 2007). Studies involving longitudinal images of muscle fibers have also taken advantage of automated image analysis methods. Computation of sarcomere length has been automated using edge-detection algorithms (Infantolino et al., 2010) or the FFT (Gannier et al., 1993; Helmes et al., 1999; Weiwad et al., 2000; Ockleford et al., 2002). The FFT has also been used to calculate myofibrillar shift from longitudinal images of skeletal muscle fibers (Shah & Lieber, 2003), but to our knowledge, this is the first time FFT-derived metrics and other textural measures were used to perform regional classification within such images. Our classification method could prove time saving in future experiments investigating changes in sarcomere length, myofibrillar phase shift, and other measures caused by manipulation of specimens prepared in a similar manner. This classification method can also be used in other fields to select for image areas of high quality and a certain periodicity. The approach simply requires creation of a series of metrics from an ROI and "training" against expertly classified ROIs. This approach may therefore prove generally useful in the study of the dynamic properties of cytoskeletal structures.

SUMMARY

Here we describe a method that provides objective classification of ROIs of striated cytoskeletal structures into usable and unusable categories. This method uses a boosted neural network, which is trained on researchers' decisions using textural parameters from the images themselves. Together these methods allow efficient, objective, and accurate classification of image regions and allow us to overcome some of the difficulties of analyzing confocal images of transfected skeletal muscle tissue.

ACKNOWLEDGMENTS

REFERENCES

Barash, I.A., Mathew, L., Ryan, A.F., Chen, J. & Lieber, R.L. (2004). Rapid muscle-specific gene expression changes after a single bout of eccentric contractions in the mouse. *Am J Physiol* **286**(2), C355–C364.

Bergen, J., Anandan, P., Hanna, K. & Hingorani, R. (1992). Hierarchical model-based motion estimation. *Proceedings of the Second European Conference on Computer Vision*, pp. 237–252. Berlin: Springer-Verlag.

Desoky, A.H. & Hall, S.A. (1990). Entropy measures for texture analysis based on Hadamard transform. *Proc IEEE Southeastcon*, vol. 462, pp. 467–470.

Eilbert, J.L., Gallistel, C.R. & McEachron, D.L. (1990). The variation in user drawn outlines on digital images: Effects on quantitative autoradiography. *Comput Med Imaging Graph* **14**(5), 331–339.

Freund, Y. & Schapire, R.E. (1996). Game theory, on-line prediction and boosting. *Proceedings of the Ninth Annual Conference on Computational Learning Theory*, pp. 325–332. Italy: Desenzano del Garda.

Gannier, F., Bernengo, J.C., Jacquemond, V. & Garnier, D. (1993). Measurements of sarcomere dynamics simultaneously with auxotonic force in isolated cardiac cells. *IEEE Trans Biomed Eng* **40**(12), 1226–1232.

Gautel, M. (2011). The sarcomeric cytoskeleton: Who picks up the strain? *Curr Opin Cell Biol* **23**(1), 39–46.

Haralick, R.M. (1979). Statistical and structural approaches to texture. *Proceedings of the IEEE* **67**(5), 786–804.

Helmes, M., Trombitas, K., Centner, T., Kellermayer, M., Labeit, S., Linke, W.A. & Granzier, H. (1999). Mechanically driven contour-length adjustment in rat cardiac titin's unique N2B sequence: titin is an adjustable spring. *Circ Res* **84**(11), 1339–1352.

Imanaka-Yoshida, K., Sanger, J.M. & Sanger, J.W. (1993). Contractile protein dynamics of myofibrils in paired adult rat cardiomyocytes. *Cell Motil Cytoskeleton* **26**(4), 301–312.

Infantolino, B.W., Ellis, M.J. & Challis, J.H. (2010). Individual sarcomere lengths in whole muscle fibers and optimal fiber length computation. *Anat Record* **293**(11), 1913–1919.

Kayser, K., Gortler, J., Bogovac, M., Bogovac, A., Goldmann, T., Vollmer, E. & Kayser, G. (2009). AI (artificial intelligence) in histopathology—From image analysis to automated diagnosis. *Folia Histochem Cytobiol* **47**(3), 355–361.

Kim, Y.-J., Brox, T., Feiden, W. & Weickert, J. (2007). Fully automated segmentation and morphometrical analysis of muscle fiber images. *Cytom Part A* **71**(1), 8–15.

Klemenčič, A., Kovačič, S. & Pernuš, F. (1998). Automated segmentation of muscle fiber images using active contour models. *Cytometry* **32**(4), 317–326.

Kueh, H.Y., Brieher, W.M. & Mitchison, T.J. (2010). Quantitative analysis of actin turnover in listeria comet tails: Evidence for catastrophic filament turnover. *Biophys J* **99**(7), 2153–2162.

Milner, D.J., Weitzer, G., Tran, D., Bradley, A. & Capetanaki, Y. (1996). Disruption of muscle architecture and myocardial degeneration in mice lacking desmin. *J Cell Biol* **134**(5), 1255–1270.

Ockleford, C.D., Cairns, H., Rowe, A.J., Byrne, S., Scott, J.J. & Willingale, R. (2002). The distribution of caveolin-3 immunofluorescence in skeletal muscle fibre membrane defined by dual channel confocal laser scanning microscopy, fast Fourier transform and image modelling. *J Microsc* **206**(Pt 2), 93–105.

PALMISANO, M.G., BREMNER, S.N., SHAH, S., RYAN, A.F. & LIEBER, R.L. (2007). Rescue of mechanical function in desmin knockout muscles by plasmid transfection. *Proceedings of the Orthopaedic Research Society Annual Conference*. San Diego, CA: ORS.

PORTNEY, L.G. & WATKINS, M.P. (1993). *Foundations of Clinical Research: Applications to Practice*. Upper Saddle River, NJ: Prentice Hall.

SHAH, S.B., DAVIS, J., WEISLEDER, N., KOSTAVASSILI, I., McCULLOCH, A.D., RALSTON, E., CAPETANAKI, Y. & LIEBER, R.L. (2004). Structural and functional roles of desmin in mouse skeletal muscle during passive deformation. *Biophys J* **86**(5), 2993–3008.

SHAH, S.B. & LIEBER, R.L. (2003). Simultaneous imaging and functional assessment of cytoskeletal protein connections in passively loaded single muscle cells. *J Histochem Cytochem* **51**(1), 19–29.

TZEKIS, P., PAPASTERGIOU, A., HATZIGAIDAS, A. & CHEVA, A. (2007). A sophisticated edge detection method for muscle biopsy image analysis. *Proceedings of the 7th WSEAS International Conference on Signal, Speech and Image Processing*. Beijing, China: World Scientific and Engineering Academy and Society.

UNSER, M. (1986). Local linear transforms for texture measurements. *Sign Process* **11**(1), 61–79.

UNSER, M. (1995). Texture classification and segmentation using wavelet frames. *IEEE Trans Image Process* **4**(11), 1549–1560.

VITADELLO, M., SCHIAFFINO, M.V., PICARD, A., SCARPA, M. & SCHIAFFINO, S. (1994). Gene transfer in regenerating muscle. *Hum Gene Ther* **5**(1), 11–18.

WEIBEL, E.R. (1980). Practical methods for biological morphometry. In *Stereological Methods*. New York: Academic Press.

WEIWAD, W.K., LINKE, W.A. & WUSSLING, M.H. (2000). Sarcomere length-tension relationship of rat cardiac myocytes at lengths greater than optimum. *J Mol Cell Cardiol* **32**(2), 247–259.

ZOU, M. & WANG, D. (2001). Texture identification and image segmentation via Fourier transform. In *Image Extraction, Segmentation, and Recognition*, pp. 34–39. Wuhan, China: SPIE.